PCCP

PAPER

View Article Online
View Journal | View Issue

Cite this: *Phys. Chem. Chem. Phys.*, 2018, **20**, 4571

Solvation effects on the vibrational modes in hydrated bicarbonate clusters

Xiangtao Kong,†[ab] Shou-Tian Sun,†[a] Ling Jiang *[b] and Zhi-Feng Liu*[ac]

Received 14th December 2017,
Accepted 12th January 2018

DOI: 10.1039/c7cp08382c

rsc.li/pccp

$HCO_3^-(H_2O)_n$ clusters provide a model system to understand the solvation interaction between the bicarbonate ion and water. Based on harmonic analysis, *ab initio* molecular dynamics simulations, and comparison with infrared multiple photon dissociation spectra and with previous results on $H_2PO_4^-(H_2O)_n$, the solvation effects on the vibrational modes of $HCO_3^-(H_2O)_n$ are analyzed. Hydrogen bond interactions have a significant impact on the vibration, especially when a hydrogen atom is directly involved in a particular mode. The COH bending mode is flattened, when the COH group is solvated by water molecules. The emergence of broad water libration modes indicates the aggregation of water molecules and the formation of a surface structure with bicarbonate on the surface.

1. Introduction

Bicarbonate (HCO_3^-) is a naturally occurring ion, observed often as an intermediate when carbon dioxide or carbonate is dissolved in water, and found to play a significant role in processes such as geochemical transformations,[1] cloud nucleation,[2] pH homeostasis in oceans,[3] CO_2 transportation, pH regulation in blood,[4–6] and skeleton formation by calcifying organisms.[7] Experimentally, its structure has been established in the solid phase by X-ray crystallography.[8] In the gas phase, its thermo-chemical properties have been measured by mass spectrometry and spectroscopy[9,10] and its electronic structure by photoelectron spectroscopy.[11] In aqueous solution, vibrational spectra have been reported for the dilute solution of $KHCO_3$ and $KDCO_3$,[12,13] indicating C_1 symmetry for the hydrated HCO_3^-. Theoretical studies have been more concerned with the solvation of HCO_3^- with water molecules. While the reaction between CO_2 and OH^- to form HCO_3^- is barrierless in the gas phase, there is a barrier around 13 kcal mol^{-1} in solution, which has been the subject of several studies.[14–19] The reaction between CO_2 and H_2O to form carbonic acid also involves HCO_3^- as an intermediate.[20] For the solvation of HCO_3^- in bulk solution, molecular dynamics studies either based on empirical potential[21] or density functional theory (DFT)[22,23] have also been reported.

More microsolvation details have been provided by studies on the hydrated bicarbonate clusters, $HCO_3^-(H_2O)_n$. Measurement by high-pressure spectroscopy provided the stepwise solvation enthalpy, at 15.7 kcal mol^{-1} for $n = 1$ decreasing to 13.4 kcal mol^{-1} at $n = 3$, and also the stepwise solvation entropy.[24] The binding energy for the negative charge was measured by photoelectron spectroscopy.[25] This shifted gradually from 4.15 eV to 6.95 eV, as n was increased from 1 to 10, and stayed around 6.95 eV for $n > 10$. The geometrical structures of $HCO_3^-(H_2O)_n$ were directly probed by infrared multiple photon dissociation (IRMPD) spectroscopy, which showed significant changes in the vibrational features between 600–1800 cm^{-1} with the increase of cluster size.[26]

However, interpreting the experimentally observed size-dependent changes is less straightforward. Similar to other hydrated cluster ions, the potential energy surface for $HCO_3^-(H_2O)_n$ is flat, and at each cluster size, there are several isomers lying close to each other in energy. The number of these isomers increases fast as the cluster size grows, which has been extensively explored in theory by the basin-hopping method in the case of $HCO_3^-(H_2O)_n$.[25] Identifying the global minimum is difficult, and neither the photoelectron nor the IRMPD spectrum at a particular size could be explained satisfactorily based on one single isomer.[25,26] As demonstrated recently in the IRMPD study of $H_2PO_4^-(H_2O)_n$,[27,28] more than one isomer could contribute to an experimental spectrum, which could be further complicated by the significant fluctuation in hydrogen bond (HB) distances and the transformation among various structures at finite temperature.

In this paper, we report a computational study on $HCO_3^-(H_2O)_n$, using both harmonic analysis and the *ab initio* molecular dynamics (AIMD) method to analyze the solvation

[a] *Department of Chemistry and Centre for Scientific Modeling and Computation, Chinese University of Hong Kong, Shatin, Hong Kong, China. E-mail: zfliu@cuhk.edu.hk*
[b] *State Key Laboratory of Molecular Reaction Dynamics, Collaborative Innovation Center of Chemistry for Energy and Materials (iChEM), Dalian Institute of Chemical Physics, Chinese Academy of Sciences, 457 Zhongshan Road, Dalian 116023, China. E-mail: ljiang@dicp.ac.cn*
[c] *CUHK Shenzhen Research Institute, No. 10, 2nd Yuexing Road, Nanshan District, Shenzhen, China*
† These authors contributed equally to this work.

dynamics and its effect on the vibration modes of HCO_3^-. Our results provide an account of the trends observed in the IRMPD spectra and also identify the evolution towards a surface cluster structure as responsible for the constant binding energy observed in the photoelectron spectra.

2. Computational methods

Two computational methods are employed in the current study. For energy optimization and the calculation of harmonic frequencies, we use the MP2 method implemented in the Gaussian 03 package,[29] with a basis set of 6-311+G(d,p) to account for the polarizability of the hydrated anion. The optimized structures are verified either as a minimum or transition structure by the absence or presence of one imaginary frequency. A scaling factor of 0.970 is used in the 600–1800 cm^{-1} region.[26,30] Calculated harmonic frequencies and intensities are convoluted using a Gaussian line shape function with a full width at half-maximum (fwhm) of 15 cm^{-1}. Zero-point corrections are added to all the relative energy values.

For the AIMD simulations, the electronic energy and atomic forces are calculated within the framework of density functional theory (DFT), while the atomic motion is treated by Newtonian mechanics, as implemented in the CP2K package.[31] The wave functions are represented by double-zeta Gaussians, and the electron density is represented by using a mixed basis set of Gaussians and auxiliary plane waves,[32] with an energy cutoff at 400 Rydberg. Goedecker–Teter–Hutter (GTH) type pseudopotentials[33–35] and the PBE exchange and correlation functional[36] are employed in the AIMD simulations, with dispersion corrected by Grimme's D3 scheme.[37]

During the AIMD simulations, a cluster ion is put at the center of a cubic box with a length of 18 Å. The effect of the periodical charge density images is eliminated by the decoupling technique developed by Martyna and Tuckerman.[38] The convergence criterion for the DFT calculation at each time step is set to 10^{-7} a.u. to guarantee the total energy conservation. The AIMD simulation is performed with an equilibration period of 5–6 ps with the temperature scaled to a desired value followed by a data collection run in the *NVE* ensemble (without temperature rescaling) with a time step of 0.5 fs. At 100, 150, 200, and 250 K, the duration of the trajectory is more than 20 ps. Each trajectory is cut into 10 ps intervals for Fourier transformation and then added up to produce the dipole time-correlation function (DTCF) spectrum for a specific temperature.

Hydrated clusters are bound by HBs, which are relatively weak and fairly flexible at finite temperature. Dynamic simulations are essential for sampling the solvated structures and for examining the thermal stability of a particular isomer. More importantly, the fluctuations of HBs have strong effects on the vibrations that can be captured by AIMD simulations. A vibrational spectrum can be directly simulated by the Fourier transform of the DTCF,[39]

$$\alpha(\omega) = \frac{2\pi\beta\omega^2}{3n(\omega)cV}\int_{-\infty}^{+\infty} dt \left\langle \vec{M}(t)\cdot\vec{M}(0)\right\rangle \exp(i\omega t)$$

where $\beta = 1/kT$, $n(\omega)$ is the refractive index, c is the speed of light in vacuum, V is the volume, and $\vec{M}$ is the total dipole moment of the system, calculated by the polarization including both ionic and electronic contributions.

3. Results and discussions

3.1 Hydrogen bond fluctuation in $HCO_3^-(H_2O)$

Shown in Fig. 1 are the three minimum-energy structures for $HCO_3^-(H_2O)$, together with the two transition-state (TS) structures connecting them. In agreement with previous reports,[25,26] the energy separation between these structures are small ($\sim$10 kJ mol^{-1}), while the energy barriers separating them are $\sim$12 kJ mol^{-1}. The existence of a number of isomers connected by a small energy barrier is a common feature for hydrated clusters. In the case of $HCO_3^-(H_2O)_n$, an extensive structural search has been performed by the unbiased basin-hopping method with n up to 13,[25] which found even more isomers with increasing n.

Here, we demonstrate another important consideration for $HCO_3^-(H_2O)_n$, the fluctuation of the HBs, as illustrated in the simplest case of n = 1. While there are two HBs between the water molecule and the bicarbonate anion in the 0 K structures (**1-a**, **1-b**, and **1-c**) shown in Fig. 1, one of the HB is easily broken during AIMD simulations so that the cluster is held together by means of just a single HB of C═O···HOH, similar to **1TS-ac** or **1TS-ab**.

In the case of **1-a**, such instability is due to the geometric constraint on the two HBs. When one H_2O solvates two C═O groups, the O···H–O angles are 140.6° and 146.8°, quite a large deviation from the ideal collinear alignment, although the two HB distances at 2.08 and 1.98 Å are typical. During an AIMD simulation, one HB would be broken, and the other would be

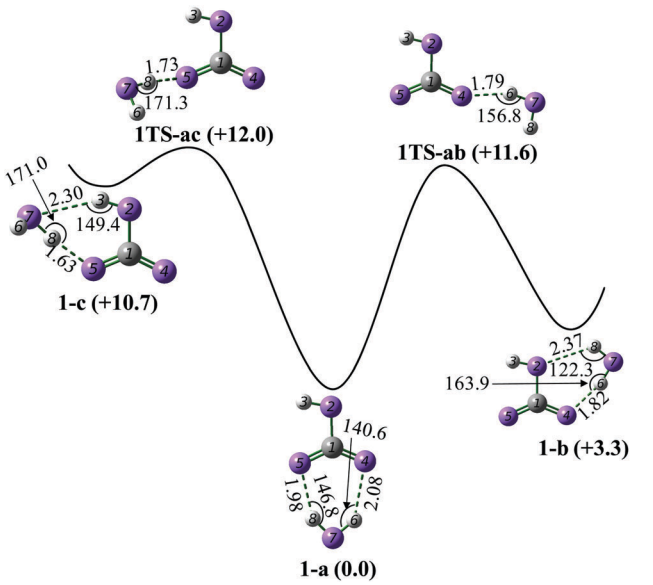

Fig. 1 Minimum-energy (**1-a**, **1-b**, and **1-c**) and transition-state (**1TS-ab** and **1TS-ac**) structures for $HCO_3^-(H_2O)$ calculated at the MP2/6-311+G(d,p) level. Relative energies (in kJ mol^{-1}) are listed inside round brackets. The distances of the hydrogen bonds are given in angstrom and the angles are given in degree.

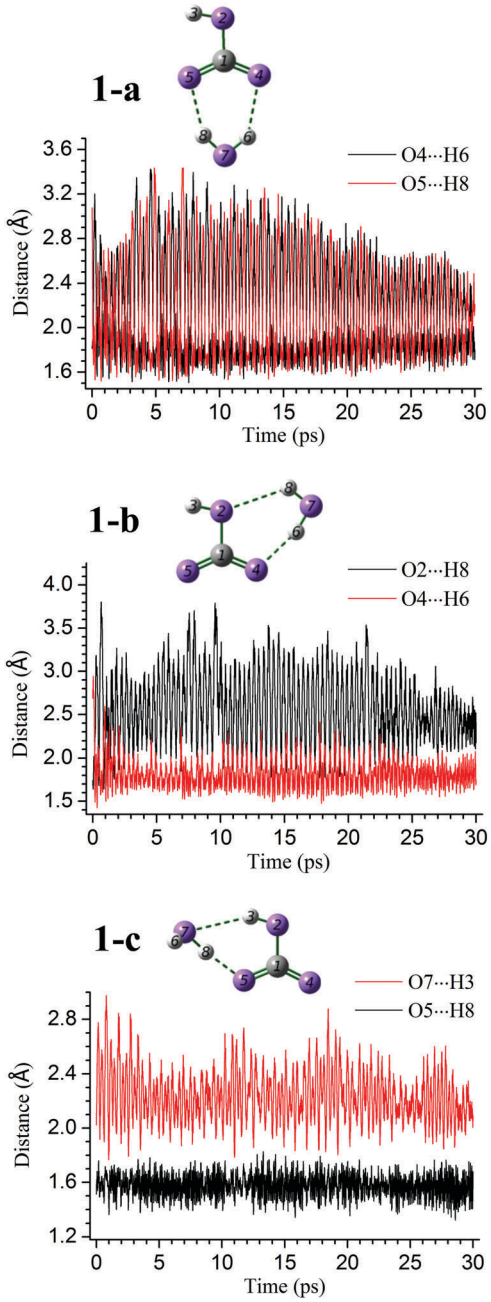

Fig. 2 Fluctuation in the HB distances during AIMD simulations at 100 K for isomers **1-a**, **1-b**, and **1-c**.

shortened to ~1.80 Å with its O···H–O angle coming closer to 180°, as shown in Fig. 2. Obviously, the breaking of one HB is compensated by the strengthening of the remaining HB.

In the case of **1-c**, when the H_2O solvate a C=O group and a C–OH group, the two HBs are quite different: the C=O···HOH distance is 1.63 Å with an O···HO angle of 171.0°, while the H_2O···HOC distance is 2.30 Å with an O···HO angle of only 149.4°. Clearly, the HB interaction is favorable for the former, but not for the latter. During AIMD simulation, the latter is easily broken. The case of **1-b** is similar to **1-c**, since it also contains one strong HB (C=O···HOH/1.82 Å/163.9°) and one weak HB (C–(H)O···HOH/2.37 Å/122.3°). During an AIMD simulation starting with any of the three isomers, there is always the significant presence of the dangling transition structures, in which HCO_3^- and H_2O are bound together by just one HB, as shown in Table 1. This is true whether the simulation temperature is 100, 150, or 200 K.

Table 1 Isomer populations (in %) for minimum-energy (**1-a**, **1-b**, and **1-c**) and transition-state (**1TS-ab** and **1TS-ac**) structures from AIMD simulations at 100, 150 K, and 200 K. The threshold distance value of the hydrogen bond is 2.40 Å

	1-a			**1-b**			**1-c**		
	100 K	150 K	200 K	100 K	150 K	200 K	100 K	150 K	200 K
1-a	42.5	63.5	46.5	0	57.3	0	0	80.7	0
1-b	0	0	0	37.8	0	35.7	0	0	0
1-c	0	0	0	0	0	0	81.9	0	72.8
1TS-ab	27.5	15.4	23.6	61.6	21.6	63.3	0	7.2	0
1TS-ac	30.0	21.1	29.9	0	21.1	0	18.1	12.1	27.2

Such a mixture of various structures has been demonstrated recently in the case of $H_2PO_4^-(H_2O)$,[27] and the O–H stretching feature is found to be very sensitive to the strength of the HB, providing strong indications for the presence of various isomers, even at a very low experimental temperature. In the previous IRMPD study on $HCO_3^-(H_2O)_n$, only the backbone region below 2000 cm^{-1} was measured.[26] The O–H stretching region for $HCO_3^-(H_2O)$ could be an interesting comparison to that for $H_2PO_4^-(H_2O)$, as the energy differences and barriers separating various isomers are higher for $HCO_3^-(H_2O)$, which could induce changes in the intensity of various O–H stretching peaks. Based on the potential energy surface shown in Fig. 1 and the comparison between theory and experiment discussed below, $HCO_3^-(H_2O)$ could be a mixture of **1-a** and **1-b**, with minor contributions from **1-c**.

3.2 HOH scissoring and COH bending

For $HCO_3^-(H_2O)_n$, the fluctuation of HB distances could also have significant effects on the two bending modes, HOH scissoring in H_2O ($\delta_{(HOH)}$) and COH bending in HCO_3^- ($\delta_{(COH)}$), since both involve a hydrogen atom that could participate in HB interaction. It has been demonstrated in the case of $H_2PO_4^-(H_2O)$ that $\delta_{(HOH)}$ is broadened to a flat feature and well reproduced by AIMD simulations.[27,28] In the case of $HCO_3^-(H_2O)$, $\delta_{(HOH)}$ contributes to feature F at around 1700 cm^{-1} as shown in Fig. 3.[26] This peak is more pronounced for $HCO_3^-(H_2O)$ than for $H_2PO_4^-(H_2O)$, with a hint of doublet splitting, due to a coincidence: there is an overlap between $\delta_{(HOH)}$ and the asymmetric C=O stretching ($\nu_{a(C=O)}$).

The COH bending is affected only when it forms an HB as a donor, as in **1-c**, which pushes $\delta_{(COH)}$ (peak D) to the blue by 50 cm^{-1} (Fig. 3). For all the other stable and transition structures, the variation in $\delta_{(COH)}$ is quite small, within 10 cm^{-1}, which is narrower than the width of peak D observed in experiment. Based on the comparison of the experimental spectrum to the calculated harmonic vibrational spectrum, it has been concluded that **1-c** does not make a significant contribution to the experimental spectrum.[26]

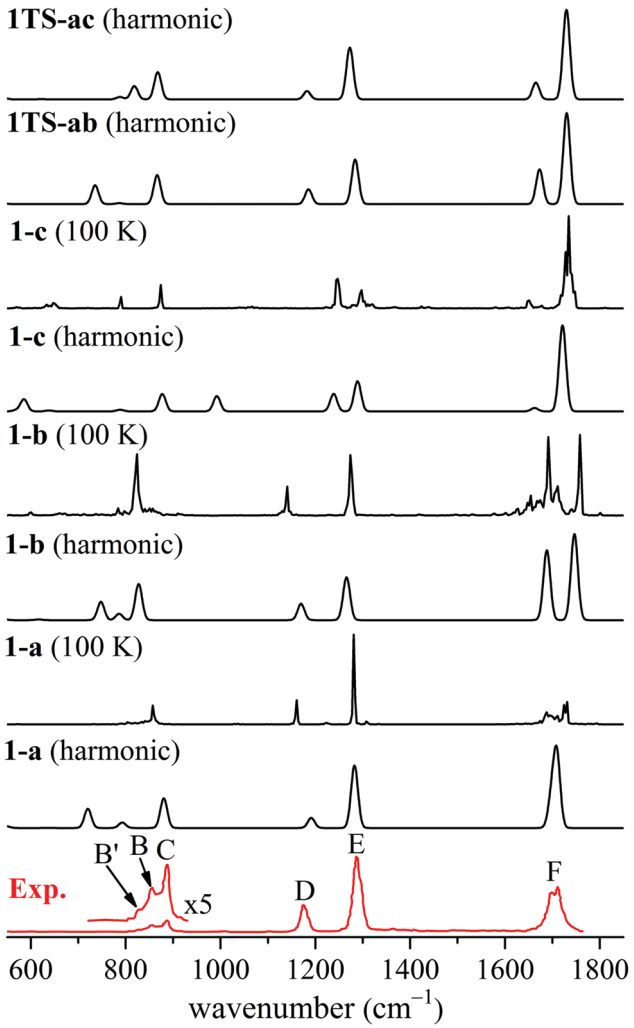

Fig. 3 Vibrational spectra for the structures shown in Fig. 1. The experimental spectrum at the bottom was provided by Prof. Knut R. Asmis. The harmonic spectra are obtained at the MP2/6-311+G(d,p) level. The spectra labeled by 100 K are obtained by the DTCF produced by AIMD simulations.

The significant gap between the $\delta_{(COH)}$ modes of **1-c** and **1-a**/**1-b** raises another important consideration, the position of $\delta_{(COH)}$ in **1-c** could be sensitive to the dynamic fluctuation of the distance of the HB in which the COH group is the donor. As demonstrated in the case of $H_2PO_4^-(H_2O)_n$,[28] such an effect could flatten the corresponding $\delta_{(POH)}$ peak. To examine it, we calculate the change in the harmonic frequency of $\delta_{(COH)}$ while constraining the COH donor HB in **1-c** to a specific distance. Such a procedure is justified by the fact that the HB is relatively weak and its fluctuation frequency (2–3 THz based on Fig. 2) is considerably slower than that of $\delta_{(COH)}$ (1200 cm^{-1}/36 THz). As shown in Fig. 4A, the $\delta_{(COH)}$ shifts by more than 100 cm^{-1} as the HB changes from 2.1 to 2.6 Å, while the shift for $\nu_{s(C=O)}$ is ~40 cm^{-1}. This indicates a significant broadening of $\delta_{(COH)}$, although the DTCF spectrum obtained at 100 K for **1-c** in Fig. 3 still shows a well-resolved peak, probably due to the low simulation temperature. Unfortunately, **1-c** is transformed into other structures when the temperature is raised to 150 K, which supports the previous conclusion that there is no significant presence of **1-c**.

As the cluster size grows, the water molecule accepting COH would be further bound to other water molecules, rather than to the C=O group in **1-c**. As shown in Fig. 4B for the **8-a** structure with n = 8, the COH···OH$_2$ HB (O19···H3) is shortened to 1.98 Å. As the HB distance is changed from 1.8 to 2.2 Å, the shift in $\delta_{(COH)}$ is 65 cm^{-1} (Fig. 4B). This is smaller than the shift for **1-c**, but comparable to the shift calculated before in the case of $H_2PO_4^-(H_2O)_n$,[28] and large enough to flatten the $\delta_{(COH)}$ peak.

Indeed, it is observed in experiment that peak D becomes almost invisible at n = 8 and beyond.[26] It means that at such sizes, there are enough water molecules around HCO_3^- so that the COH group is always solvated by a donor HB. As a result, peak D disappears as $\delta_{(COH)}$ is flattened by the fluctuation in this HB distance.

3.3 C=O stretching

The symmetric C=O stretching (feature E) is an example of a vibrational mode which is less affected by the solvation interaction. Although the O atoms do form HBs, $\nu_{s(C=O)}$ involves two atoms much heavier than H and is less sensitive to the fluctuation in HB distance. The shift in $\nu_{s(C=O)}$, shown in Fig. 4, is indeed significantly smaller than the shift in $\delta_{(COH)}$ when the distance of the COH donor HB is varied. As n increases from 1 to 10, the $\nu_{s(C=O)}$ peak position shifts to the blue by ~60 cm^{-1} in the experimental spectra,[26] while its shape changes little. In our previous study on $H_2PO_4^-(H_2O)_n$, the symmetric P=O stretching also changes little in its shape as n increases from 1 to 12, although the peak positions shifts in the opposite direction, by ~15 cm^{-1} to the red.[27] This indicates that while the P=O bonds in $H_2PO_4^-$ are slightly weakened by solvation, the C=O bonds in HCO_3^- are strengthened by solvation.

The $\nu_{a(C=O)}$ frequency in $HCO_3^-(H_2O)_n$ happens to be very close to $\delta_{(HOH)}$. Dynamic broadening is expected to be important for the latter, but not for the former. Furthermore, harmonic calculations indicate significant coupling between these two modes, making it difficult to extract structural information from the fairly broad peak F. For future experiments, it would be interesting to measure the IRMPD spectra for $DCO_3^-(D_2O)_n$, in which the $\nu_{a(C=O)}$ and $\delta_{(DOD)}$ modes could be separated.

3.4 C–OH stretching and CO_3 out-of-plane bending

Below 1000 cm^{-1}, the experimentally observed features have been assigned to C–OH stretching ($\nu_{(C-OH)}$, peak C), CO_3 out-of-plane bending ($\gamma_{(CO_3)}$, peak B), and various H_2O libration modes (broad feature A, shown in Fig. 1, ref. 26), with feature A only becoming more prominent for the $n \geq 6$ clusters.[26] Among these three modes, $\gamma_{(CO_3)}$ is the least sensitive to solvation. At n = 1, the calculated harmonic frequency is 794 cm^{-1} for **1-a**, 782 cm^{-1} for **1-b**, 788 cm^{-1} for **1-c**, within a gap of only 12 cm^{-1}, and these are also very close to the value of 787 cm^{-1} for the bare HCO_3^-. As n increases, the calculated $\gamma_{(CO_3)}$ shifts to the blue, to ~840 cm^{-1} at n = 4, and ~850 cm^{-1} at n = 7, in agreement with the small blue-shift observed in the experiment.

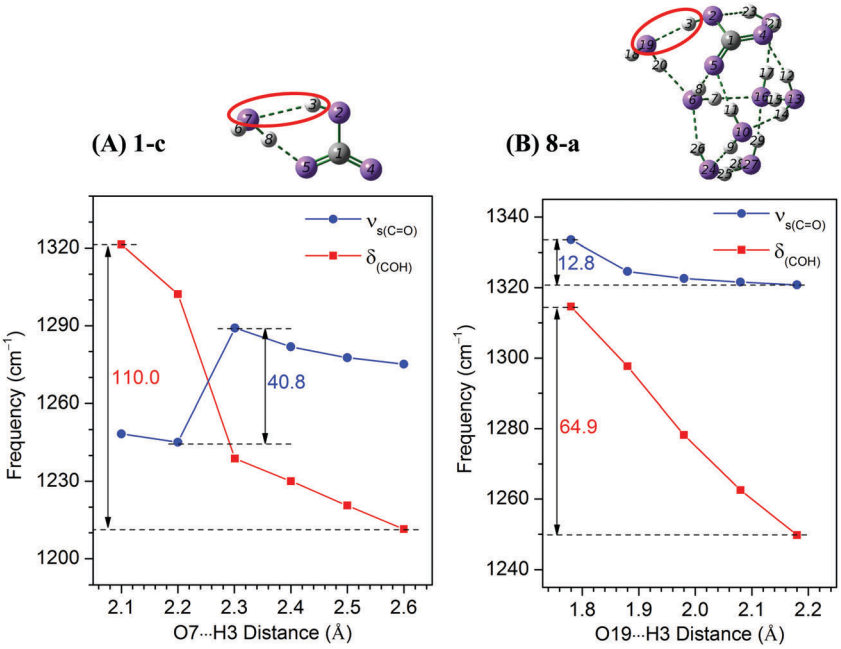

Fig. 4 The $\nu_{s(C=O)}$ and $\delta_{(COH)}$ frequencies as a function of COH donor HB distance for **1-c** (O7···H3 distance) (A) and **8-a** (O19···H3 distance) (B) obtained at the MP2/6-311+G(d,p) level.

The only problem is with the case of $n = 1$. The peak at 859 cm^{-1} in $n = 1$ (labeled peak B in Fig. 3) is significantly higher than that of the peak positions of $\gamma_{(CO_3)}$ in n = 2–10 (826–841 cm^{-1}).[26] Considering that its calculated position is blue-shifted to only 850 cm^{-1} by $n = 7$, the peak at 859 cm^{-1} in the $n = 1$ experimental spectrum is unlikely to be due to $\gamma_{(CO_3)}$, as previously assigned. Instead, $\gamma_{(CO_3)}$ should be assigned to the lower frequency tail, labeled as B′ in Fig. 3.

The C–OH stretching mode ($\nu_{(C-OH)}$) is sensitive to the position of H_2O. In the case of $n = 1$, the calculated $\nu_{(C-OH)}$ is 880 cm^{-1} for **1-a**, 877 cm^{-1} for **1-c**, and 827 cm^{-1} for **1-b**. In the experimental IRMPD spectrum of $n = 1$,[26] the peaks at 859 cm^{-1} (peak B) and 887 cm^{-1} (peak C) could both be assigned to $\nu_{(C-OH)}$, indicating that $HCO_3^-(H_2O)$ could well be a mixture of **1-a** and **1-b**. As n increases, the calculated $\nu_{(C-OH)}$ shows a trend of shifting to higher frequency while the frequency gap between various isomers is reduced. This is in good agreement with the experimentally observed blue shift and better resolved shape for peak C, as n increases from 2 to 7. The further broadening of this peak for n above 7 is due its coupling with the numerous libration modes of H_2O as n increases.

3.5 Libration modes and surface cluster

The libration modes of water produce a broad feature labeled as A in the experimental report,[26] centering around 700 cm^{-1} and extending all the way up to 1000 cm^{-1}. Its intensity is size sensitive, being appreciable only at $n = 6$ and above, and increasing further with the cluster size. These modes are known to be sensitive to the fluctuation in the HB network, and for bulk samples, related to long range and collective motions.[40–42] Reproducing peak A would require detailed AIMD simulations on the larger clusters with long durations. Nonetheless, two conclusions could be drawn by harmonic analysis and short duration AIMD simulations.

The first conclusion concerns the coupling between the libration modes with either $\nu_{(C-OH)}$ or $\gamma_{(CO_3)}$. Harmonic analysis indicates that the coupling with $\nu_{(C-OH)}$ is significant, producing several harmonic peaks, which is responsible for the broadening of peak C at $n \geq 8$. On the other hand, the coupling with $\gamma_{(CO_3)}$ is less significant, as the out-of-plane motion of a C atom does not disturb the HB network as much as the stretching of the C–OH bond. As a result, the $\gamma_{(CO_3)}$ peak (B′ for $n = 1$ and B for $n > 1$) is maintained all the way up to $n = 10$, even when its baseline is raised by the contribution from the water libration modes.

The second conclusion concerns the aggregation of the water molecule. As shown in Fig. 5, there are three solvation sites, α, β, and γ in HCO_3^-, using the labels previously employed.[26] When n is small, the water molecules on these three sites are not connected to each other by HB. However, by $n = 6$, the HB network is extensive enough such that the water molecules on these three sites are connected. In such cases, the overall structure could be characterized as a surface cluster, with water molecules aggregated below the planar bicarbonate anion. These structures are among the most stable at $n = 7$ and $n = 8$, and robust during AIMD simulations. Their presences could account for the sudden enhancement of peak A above $n = 6$,[26] which indicates the collective motion of large water aggregates.[40]

Furthermore, the emergence of the surface cluster could also explain another interesting observation in the photodetachment study on $HCO_3^-(H_2O)_n$: the vertical detachment energy (VDE) increases gradually with n and becomes a constant of 6.95 eV for $n \geq 9$.[11] When HCO_3^- is on the surface, additional water molecules would aggregate at the bottom in the third or

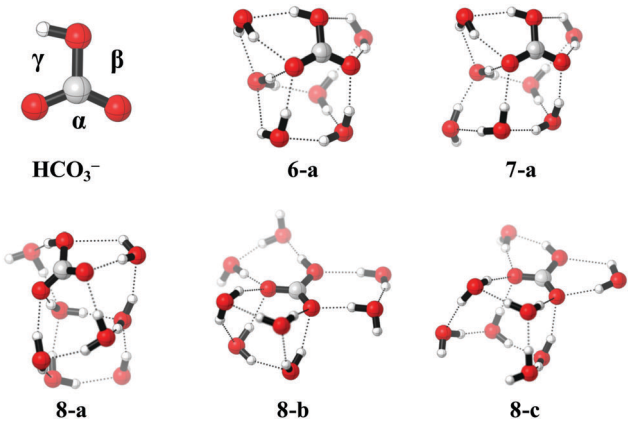

Fig. 5 Lowest-energy isomers of $HCO_3^-(H_2O)_n$ (n = 6–8) optimized by MP2/6-311+G(d,p) and position labelling used in the Results and discussion section. **7-a** and **8-a** are surface clusters, with HCO_3^- laying flat at the cluster surface.

higher solvation shell, which is far away from the bicarbonate anion and have little effect on the VDE of the negative charge.

3.6 DTCF spectra for n = 6

Shown in Fig. 6 are the DTCF spectra for three isomers with n = 6, obtained by AIMD simulations. The calculated spectra are dependent on the simulation temperature, and also on the starting geometry, indicating that a much longer simulation period would be needed to fully reproduce the experimental features. However, dynamic features can be discerned from these spectra.

6-a is a surface cluster, although at n = 6, it is not yet the most stable isomer. During AIMD simulation at 200 K, it is often transformed into a structure with only one water molecule at the γ site. As expected, the $\delta_{(COH)}$ is blue shifted to the position just below peak E and broadened, providing an example for the disappearance of peak D.

For **6-b**, there is one water molecule on each of the β and γ sites. However, during AIMD simulation, **6-b** is unstable and easily transformed into **6-c** which does not have any water on the β or γ site. As a result, the simulated spectra for **6-b** and **6-c** are similar to each other. They are also similar to the experimental IRMPD spectrum, with the presence of peak D indicating that COH is not solvated yet.

For all three isomers, there are many features around 800 cm^{-1}, which should produce a broad feature, as water aggregation is observed during the AIMD simulations for all three isomers. Such a broad feature, due to the water libration modes, is indeed observed in the experimental spectrum.

3.7 Comparison between hydrated HCO_3^- and $H_2PO_4^-$ clusters

Solvation effects on the backbone vibration modes have also been studied in detail for hydrated $H_2PO_4^-$ clusters.[28] It is interesting to compare the cases of HCO_3^- and $H_2PO_4^-$ since both are polyatomic anions, with X=O and XOH (X = C and P) groups.

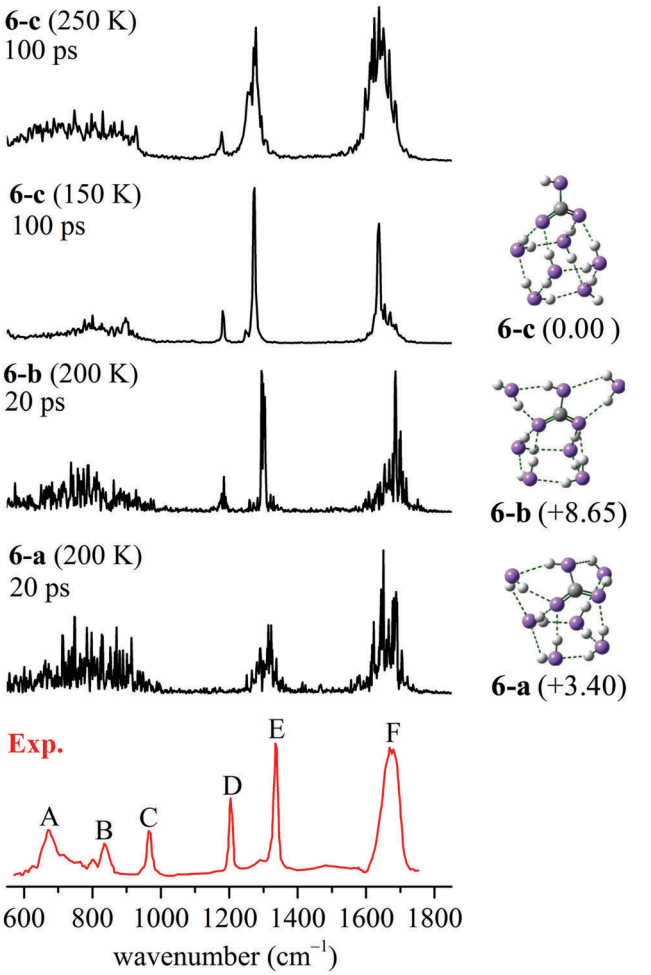

Fig. 6 DTCF spectra for three isomers of $HCO_3^-(H_2O)_6$, obtained by AIMD simulations, and compared with the experimental IRMPD spectrum provided by Prof. Knut R. Asmis. MP2/6-311+G(d,p) relative energies (in kJ mol^{-1}) are listed inside round brackets.

There are obvious similarities between these two systems. The symmetric X=O stretching is relatively stable, showing only a small shift in position with increasing cluster size. XOH bending is very sensitive to solvation, and when it is a donor for HB, it is flattened by the fluctuation in HB distance. X–OH stretching is usually resolved and shifted to the blue as more water molecules are added. HOH scissoring is always broadened due to HB fluctuation.

There are also differences. In $H_2PO_4^-(H_2O)_n$, the asymmetric X=O stretching is coupled with X–OH bending, while in $HCO_3^-(H_2O)_n$, it is coupled with HOH bending. There is a well-resolved out-of-plane peak for $HCO_3^-(H_2O)_n$, while $H_2PO_4^-(H_2O)_n$ is tetrahedral. As the cluster size grows, the symmetric X=O stretching peak moves to the red in $H_2PO_4^-(H_2O)_n$ and to the blue in $HCO_3^-(H_2O)_n$.

The most interesting contrast is in the aggregation of solvent water molecules. HCO_3^- is planar, and water molecules can aggregate on one side of the plane, starting at a modest size of n = 6 and producing a surface cluster. In the IRMPD spectra, the libration modes of water shows up prominently at n = 6, and in

the photo-detachment spectra, VDE becomes a constant for $n \geq 9$.[11] $H_2PO_4^-$ is tetrahedral and has one more XOH group than HCO_3^-, and more water molecules are required for the onset of solvent aggregation. In fact, the water libration feature for $H_2PO_4^-(H_2O)_n$, which is also a broad feature centered around 700 cm^{-1}, does not show much intensity until n reaches 12.[28] Accordingly, one would expect the VDE of $H_2PO_4^-(H_2O)_n$ to shift to a higher energy beyond n = 12.

4. Summary

Understanding the IRMPD spectra of $HCO_3^-(H_2O)_n$ requires the consideration of more than one isomer and the fluctuation of HB distances. Vibrational modes with the involvement of a hydrogen atom participating in HB are most affected, such as OH stretching, COH or HOH bending, and water libration. In the backbone region, this is demonstrated by the flattening of the COH bending peak for $n \geq 8$, which indicates that the COH group is solvated at such sizes for all the isomers present. For the other vibrational modes, the increasing extent of solvation with growing cluster size only induces shifts in peak positions. The onset of the water libration feature at n = 6 indicates the early beginning of solvent aggregation, as the planar HCO_3^- stays at the surface of the cluster. The dominance of such a surface structure at larger n also accounts for the constant vertical detachment energy for $n \geq 9$.

Conflicts of interest

There are no conflicts to declare.

Acknowledgements

This work was supported by the National Natural Science Foundation of China (Grants No. 21327901, 21473151, 21673231, and 21688102), and the Key Research Program (Grant No. KGZD-EW-T05) and the Strategic Priority Research Program (Grant No. XDB17010000) of the Chinese Academy of Science. We thank Professor Knut R. Asmis for providing us the IRMPD experimental spectra.

References

1 K. S. Lackner, *Annu. Rev. Energy*, 2002, **27**, 193–232.
2 J. M. C. Plane, *Ann. Geophys. - Atm. Hydr.*, 2000, **18**, 807–814.
3 K. Caldeira and M. E. Wickett, *Nature*, 2003, **425**, 365.
4 D. N. Silverman and S. Lindskog, *Acc. Chem. Res.*, 1988, **21**, 30–36.
5 S. Lindskog, *Pharmacol. Ther.*, 1997, **74**, 1–20.
6 D. W. Christianson and C. A. Fierke, *Acc. Chem. Res.*, 1996, **29**, 331–339.
7 J. C. Orr, V. J. Fabry, O. Aumont, L. Bopp, S. C. Doney, R. A. Feely, A. Gnanadesikan, N. Gruber, A. Ishida, F. Joos, R. M. Key, K. Lindsay, E. Maier-Reimer, R. Matear, P. Monfray, A. Mouchet, R. G. Najjar, G. K. Plattner, K. B. Rodgers, C. L. Sabine, J. L. Sarmiento, R. Schlitzer, R. D. Slater, I. J. Totterdell, M. F. Weirig, Y. Yamanaka and A. Yool, *Nature*, 2005, **437**, 681–686.
8 B. D. Sharma, *Acta Crystallogr.*, 1965, **18**, 818–819.
9 R. R. Squires, *Int. J. Mass Spectrom.*, 1992, **117**, 565–600.
10 P. M. Hierl and J. F. Paulson, *J. Chem. Phys.*, 1984, **80**, 4890–4900.
11 X. B. Wang and S. S. Xantheas, *J. Phys. Chem. Lett.*, 2011, **2**, 1204–1210.
12 W. W. Rudolph, D. Fischer and G. Irmer, *Appl. Spectrosc.*, 2006, **60**, 130–144.
13 W. W. Rudolph, G. Irmer and E. Konigsberger, *Dalton Trans.*, 2008, 900–908.
14 B. Jonsson, G. Karlstrom and H. Wennerstrom, *J. Am. Chem. Soc.*, 1978, **100**, 1658–1661.
15 J. Y. Liang and W. N. Lipscomb, *J. Am. Chem. Soc.*, 1986, **108**, 5051–5058.
16 Z. Peng and K. M. Merz, *J. Am. Chem. Soc.*, 1993, **115**, 9640–9647.
17 M. M. Davidson, I. H. Hillier, R. J. Hall and N. A. Burton, *Mol. Phys.*, 1994, **83**, 327–333.
18 A. V. Nemukhin, I. A. Topol, B. L. Grigorenko and S. K. Burt, *J. Phys. Chem. B*, 2002, **106**, 1734–1740.
19 K. Iida, D. Yokogawa, H. Sato and S. Sakaki, *Chem. Phys. Lett.*, 2007, **443**, 264–268.
20 A. Stirling and I. Papai, *J. Phys. Chem. B*, 2010, **114**, 16854–16859.
21 V. Vchirawongkwin, A. B. Pribil and B. M. Rode, *J. Comput. Chem.*, 2010, **31**, 249–257.
22 P. P. Kumar, A. G. Kalinichev and R. J. Kirkpatrick, *J. Phys. Chem. B*, 2009, **113**, 794–802.
23 K. Leung, I. M. B. Nielsen and I. Kurtz, *J. Phys. Chem. B*, 2007, **111**, 4453–4459.
24 R. G. Keesee, N. Lee and A. W. Castleman, *J. Am. Chem. Soc.*, 1979, **101**, 2599–2604.
25 H. Wen, G. L. Hou, Y. R. Liu, X. B. Wang and W. Huang, *Phys. Chem. Chem. Phys.*, 2016, **18**, 17470–17482.
26 E. Garand, T. Wende, D. J. Goebbert, R. Bergmann, G. Meijer, D. M. Neumark and K. R. Asmis, *J. Am. Chem. Soc.*, 2010, **132**, 849–856.
27 L. Jiang, S.-T. Sun, N. Heine, J.-W. Liu, T. I. Yacovitch, T. Wende, Z.-F. Liu, D. M. Neumark and K. R. Asmis, *Phys. Chem. Chem. Phys.*, 2014, **16**, 1314–1318.
28 S. T. Sun, L. Jiang, J. W. Liu, N. Heine, T. I. Yacovitch, T. Wende, K. R. Asmis, D. M. Neumark and Z. F. Liu, *Phys. Chem. Chem. Phys.*, 2015, **17**, 25714–25724.
29 M. J. Frisch, G. W. Trucks, H. B. Schlegel, G. E. Scuseria, M. A. Robb, J. R. Cheeseman, J. A. Montgomery, T. Vreven Jr, K. N. Kudin, J. C. Burant, J. M. Millam, S. S. Iyengar, J. Tomasi, V. Barone, B. Mennucci, M. Cossi, G. Scalmani, N. Rega, G. A. Petersson, H. Nakatsuji, M. Hada, M. Ehara, K. Toyota, R. Fukuda, J. Hasegawa, M. Ishida, T. Nakajima, Y. Honda, O. Kitao, H. Nakai, M. Klene, X. Li, J. E. Knox, H. P. Hratchian, J. B. Cross, V. Bakken, C. Adamo, J. Jaramillo, R. Gomperts, R. E. Stratmann, O. Yazyev, A. J. Austin, R. Cammi, C. Pomelli, J. W. Ochterski, P. Y. Ayala, K. Morokuma, G. A. Voth, P. Salvador, J. J. Dannenberg, V. G. Zakrzewski, S. Dapprich, A. D. Daniels, M. C. Strain, O. Farkas, D. K. Malick, A. D. Rabuck, K. Raghavachari,

J. B. Foresman, J. V. Ortiz, Q. Cui, A. G. Baboul, S. Clifford, J. Cioslowski, B. B. Stefanov, G. Liu, A. Liashenko, P. Piskorz, I. Komaromi, R. L. Martin, D. J. Fox, T. Keith, M. A. Al-Laham, C. Y. Peng, A. Nanayakkara, M. Challacombe, P. M. W. Gill, B. Johnson, W. Chen, M. W. Wong, C. Gonzalez and J. A. Pople, *Gaussian03, revision D.01*, Gaussian, Inc., Pittsburgh, PA, 2005.

30 J. P. Merrick, D. Moran and L. Radom, *J. Phys. Chem. A*, 2007, **111**, 11683–11700.

31 J. VandeVondele, M. Krack, F. Mohamed, M. Parrinello, T. Chassaing and J. Hutter, *Comput. Phys. Commun.*, 2005, **167**, 103–128.

32 G. Lippert, J. r. Hutter and M. Parrinello, *Theor. Chem. Acc.*, 1999, **103**, 124–140.

33 M. Krack, *Theor. Chem. Acc.*, 2005, **114**, 145–152.

34 S. Goedecker, M. Teter and J. Hutter, *Phys. Rev. B: Condens. Matter Mater. Phys.*, 1996, **54**, 1703–1710.

35 C. Hartwigsen, S. Goedecker and J. Hutter, *Phys. Rev. B: Condens. Matter Mater. Phys.*, 1998, **58**, 3641–3662.

36 J. P. Perdew, K. Burke and M. Ernzerhof, *Phys. Rev. Lett.*, 1996, **77**, 3865–3868.

37 S. Grimme, J. Antony, S. Ehrlich and H. Krieg, *J. Chem. Phys.*, 2010, **132**, 154104.

38 G. J. Martyna and M. E. Tuckerman, *J. Chem. Phys.*, 1999, **110**, 2810–2821.

39 D. A. McQuarrie, *Statistic Mechanics*, Harper-Collins Publishers, New York, 1976.

40 M. Heyden, J. Sun, S. Funkner, G. Mathias, H. Forbert, M. Havenith and D. Marx, *Proc. Natl. Acad. Sci. U. S. A.*, 2010, **107**, 12068–12073.

41 M. Heyden, J. Sun, H. Forbert, G. Mathias, M. Havenith and D. Marx, *J. Phys. Chem. Lett.*, 2012, **3**, 2135–2140.

42 M. Smiechowski, J. Sun, H. Forbert and D. Marx, *Phys. Chem. Chem. Phys.*, 2015, **17**, 8323–8329.

